In vivo bioluminescence and reflectance imaging of multiple organs in bioluminescence reporter mice by bundled-fiber-coupled microscopy

Yoriko Ando,[1] Takashi Sakurai,[1,2] Kowa Koida,[1,3] Hajime Tei,[4] Akiko Hida,[5] Kazuki Nakao,[6,7] Mistuo Natsume,[8] and Rika Numano[1,9,*]

[1]*Electronics-Inspired Interdisciplinary Research Institute (EIIRIS), Toyohashi University of Technology, Toyohashi, Aichi, 441-8580, Japan*
[2]*Juntendo University, Bunkyo-ku, Tokyo, 113-8421, Japan*
[3]*Department of Computer Science and Engineering, Toyohashi University of Technology, Toyohashi, Aichi, 441-8580, Japan*
[4]*Graduate School of Natural Science and Technology, Kanazawa University, Kanazawa, Ishikawa, 920-1192, Japan*
[5]*Department of Psychophysiology, National Institute of Mental Health, National Center of Neurology and Psychiatry, Kodaira, Tokyo, 187-8553 Japan*
[6]*Laboratory of Animal Resources, Center for Disease Biology and Integrative Medicine, Graduate School of Medicine, The University of Tokyo, Bunkyo-ku, Tokyo, 113-0033, Japan*
[7]*Laboratory for Animal Resources and Genetic Engineering, RIKEN Center for Developmental Biology, Kobe, Hyogo, 650-0047, Japan*
[8]*Denkosha Co., Ltd., Hamamatsu, Shizuoka, 432-8055, Japan*
[9]*Department of Environmental and Life Science, Biological Regulatory Engineering, Toyohashi University of Technology, Toyohashi, Aichi, 441-8580, Japan*
[*]*numano@tut.jp*

Abstract: Bioluminescence imaging (BLI) is used in biomedical research to monitor biological processes within living organisms. Recently, fiber bundles with high transmittance and density have been developed to detect low light with high resolution. Therefore, we have developed a bundled-fiber-coupled microscope with a highly sensitive cooled-CCD camera that enables the BLI of organs within the mouse body. This is the first report of *in vivo* BLI of the brain and multiple organs in luciferase-reporter mice using bundled-fiber optics. With reflectance imaging, the structures of blood vessels and organs can be seen clearly with light illumination, and it allowed identification of the structural details of bioluminescence images. This technique can also be applied to clinical diagnostics in a low invasive manner.

OCIS codes: (110.2350) Fiber optics imaging; (170.2150) Endoscopic imaging; (170.3880) Medical and biological imaging.

References and links

1. C. E. Badr and B. A. Tannous, "Bioluminescence imaging: progress and applications," Trends Biotechnol. **29**(12), 624–633 (2011).
2. M. Deluca, "Firefly luciferase," Adv. Enzymol. Relat. Areas Mol. Biol. **44**, 37–68 (1976).
3. K. V. Wood, "The chemical mechanism and evolutionary development of beetle bioluminescence," Photochem. Photobiol. **62**(4), 662–673 (1995).
4. O. Shimomura, *Bioluminescence: chemical principles and methods* (World Scientific, Hackensack, N.J., 2006), pp. xxvii, 470 p.
5. T. Troy, D. Jekic-McMullen, L. Sambucetti, and B. Rice, "Quantitative comparison of the sensitivity of detection of fluorescent and bioluminescent reporters in animal models," Mol. Imaging **3**(1), 9–23 (2004).
6. A. D. Mehta, J. C. Jung, B. A. Flusberg, and M. J. Schnitzer, "Fiber optic in vivo imaging in the mammalian nervous system," Curr. Opin. Neurobiol. **14**(5), 617–628 (2004).
7. B. A. Flusberg, E. D. Cocker, W. Piyawattanametha, J. C. Jung, E. L. Cheung, and M. J. Schnitzer, "Fiber-optic fluorescence imaging," Nat. Methods **2**(12), 941–950 (2005).
8. D. Rector and R. Harper, "Imaging of hippocampal neural activity in freely behaving animals," Behav. Brain Res. **42**(2), 143–149 (1991).

9. M. Hirano, Y. Yamashita, and A. Miyakawa, "In vivo visualization of hippocampal cells and dynamics of Ca2+ concentration during anoxia: feasibility of a fiber-optic plate microscope system for in vivo experiments," Brain Res. **732**(1-2), 61–68 (1996).
10. T. Sakurai and K. Koida, "Activity-dependent neuronal signals detected by a fiber-coupled fluorescence microscopy," Proc. SPIE **8928**, 89280V (2014).
11. T. Ohigashi, N. Kozakai, R. Mizuno, A. Miyajima, and M. Murai, "Endocytoscopy: novel endoscopic imaging technology for in-situ observation of bladder cancer cells," J. Endourol. **20**(9), 698–701 (2006).
12. M. Hughes, T. P. Chang, and G. Z. Yang, "Fiber bundle endocytoscopy," Biomed. Opt. Express **4**(12), 2781–2794 (2013).
13. H. Tei, H. Okamura, Y. Shigeyoshi, C. Fukuhara, R. Ozawa, M. Hirose, and Y. Sakaki, "Circadian oscillation of a mammalian homologue of the Drosophila period gene," Nature **389**(6650), 512–516 (1997).
14. Z. S. Sun, U. Albrecht, O. Zhuchenko, J. Bailey, G. Eichele, and C. C. Lee, "RIGUI, a putative mammalian ortholog of the Drosophila period gene," Cell **90**(6), 1003–1011 (1997).
15. S. M. Reppert and D. R. Weaver, "Coordination of circadian timing in mammals," Nature **418**(6901), 935–941 (2002).
16. R. Numano, S. Yamazaki, N. Umeda, T. Samura, M. Sujino, R. Takahashi, M. Ueda, A. Mori, K. Yamada, Y. Sakaki, S. T. Inouye, M. Menaker, and H. Tei, "Constitutive expression of the Period1 gene impairs behavioral and molecular circadian rhythms," Proc. Natl. Acad. Sci. U.S.A. **103**(10), 3716–3721 (2006).
17. A. Hida, N. Koike, M. Hirose, M. Hattori, Y. Sakaki, and H. Tei, "The human and mouse Period1 genes: five well-conserved E-boxes additively contribute to the enhancement of mPer1 transcription," Genomics **65**(3), 224–233 (2000).
18. L. D. Wilsbacher, S. Yamazaki, E. D. Herzog, E. J. Song, L. A. Radcliffe, M. Abe, G. Block, E. Spitznagel, M. Menaker, and J. S. Takahashi, "Photic and circadian expression of luciferase in mPeriod1-luc transgenic mice invivo," Proc. Natl. Acad. Sci. U.S.A. **99**(1), 489–494 (2002).
19. S. Yamazaki, R. Numano, M. Abe, A. Hida, R. Takahashi, M. Ueda, G. D. Block, Y. Sakaki, M. Menaker, and H. Tei, "Resetting central and peripheral circadian oscillators in transgenic rats," Science **288**(5466), 682–685 (2000).
20. T. Yamamoto, Y. Nakahata, H. Soma, M. Akashi, T. Mamine, and T. Takumi, "Transcriptional oscillation of canonical clock genes in mouse peripheral tissues," BMC Mol. Biol. **5**(1), 18 (2004).
21. R. Matsumura, A. Okamoto, K. Node, and M. Akashi, "Compensation for intracellular environment in expression levels of mammalian circadian clock genes," Sci. Rep. **4**, 4032 (2014).
22. C. Hara-Miyauchi, O. Tsuji, A. Hanyu, S. Okada, A. Yasuda, T. Fukano, C. Akazawa, M. Nakamura, T. Imamura, Y. Matsuzaki, H. J. Okano, A. Miyawaki, and H. Okano, "Bioluminescent system for dynamic imaging of cell and animal behavior," Biochem. Biophys. Res. Commun. **419**(2), 188–193 (2012).
23. F. Lanni, A. S. Waggoner, and D. L. Taylor, "Structural organization of interphase 3T3 fibroblasts studied by total internal reflection fluorescence microscopy," J. Cell Biol. **100**(4), 1091–1102 (1985).
24. X. J. Liang, A. Q. Liu, C. S. Lim, T. C. Ayi, and P. H. Yap, "Determining refractive index of single living cell using an integrated microchip," Sens. Actuators A Phys. **133**(2), 349–354 (2007).
25. M. Nitzan, A. Romem, and R. Koppel, "Pulse oximetry: fundamentals and technology update," Med. Devices (Auckl.) **7**, 231–239 (2014).
26. A. Ago, T. Gonda, K. Kawakami, and H. Sahata, "[Morphological studies on preputial gland of mice--1. Light and transmission electron microscopic observations of preputial gland in male mice]," Exp. Anim. **43**(5), 645–649 (1995).
27. M. Keyaerts, V. Caveliers, and T. Lahoutte, "Bioluminescence imaging: looking beyond the light," Trends Mol. Med. **18**(3), 164–172 (2012).
28. Y. Tahara, H. Kuroda, K. Saito, Y. Nakajima, Y. Kubo, N. Ohnishi, Y. Seo, M. Otsuka, Y. Fuse, Y. Ohura, T. Komatsu, Y. Moriya, S. Okada, N. Furutani, A. Hirao, K. Horikawa, T. Kudo, and S. Shibata, "In vivo monitoring of peripheral circadian clocks in the mouse," Curr. Biol. **22**(11), 1029–1034 (2012).
29. W. Wang and W. S. El-Deiry, "Bioluminescent molecular imaging of endogenous and exogenous p53-mediated transcription in vitro and in vivo using an HCT116 human colon carcinoma xenograft model," Cancer Biol. Ther. **2**(2), 196–202 (2003).
30. M. Keyaerts, J. Verschueren, T. J. Bos, L. O. Tchouate-Gainkam, C. Peleman, K. Breckpot, C. Vanhove, V. Caveliers, A. Bossuyt, and T. Lahoutte, "Dynamic bioluminescence imaging for quantitative tumour burden assessment using IV or IP administration of D: -luciferin: effect on intensity, time kinetics and repeatability of photon emission," Eur. J. Nucl. Med. Mol. Imaging **35**(5), 999–1007 (2008).
31. G. Keiser, F. Xiong, Y. Cui, and P. P. Shum, "Review of diverse optical fibers used in biomedical research and clinical practice," J. Biomed. Opt. **19**(8), 080902 (2014).
32. J. Sun, C. Shu, B. Appiah, and R. Drezek, "Needle-compatible single fiber bundle image guide reflectance endoscope," J. Biomed. Opt. **15**(4), 040502 (2010).
33. X. Liu, Y. Huang, and J. U. Kang, "Dark-field illuminated reflectance fiber bundle endoscopic microscope," J. Biomed. Opt. **16**(4), 046003 (2011).
34. M. Hughes, P. Giataganas, and G. Z. Yang, "Color reflectance fiber bundle endomicroscopy without back-reflections," J. Biomed. Opt. **19**(3), 030501 (2014).
35. D. T. Moore, "Gradient-index optics: a review," Appl. Opt. **19**(7), 1035–1038 (1980).
36. B. E. A. Saleh and M. C. Teich, *Fundamentals of Photonics* (John Wiley & Sons, Inc., New York, USA, 1991).
37. J. Knittel, L. Schnieder, G. Buess, B. Messerschmidt, and T. Possner, "Endoscope-compatible confocal microscope using a gradient index-lens system," Opt. Commun. **188**(5-6), 267–273 (2001).

38. J. C. Jung, A. D. Mehta, E. Aksay, R. Stepnoski, and M. J. Schnitzer, "In vivo mammalian brain imaging using one- and two-photon fluorescence microendoscopy," J. Neurophysiol. **92**(5), 3121–3133 (2004).

39. J. M. Jabbour, M. A. Saldua, J. N. Bixler, and K. C. Maitland, "Confocal endomicroscopy: instrumentation and medical applications," Ann. Biomed. Eng. **40**(2), 378–397 (2012).

40. S. T. Adams, Jr. and S. C. Miller, "Beyond D-luciferin: expanding the scope of bioluminescence imaging in vivo," Curr. Opin. Chem. Biol. **21**, 112–120 (2014).

41. K. Saito, Y. F. Chang, K. Horikawa, N. Hatsugai, Y. Higuchi, M. Hashida, Y. Yoshida, T. Matsuda, Y. Arai, and T. Nagai, "Luminescent proteins for high-speed single-cell and whole-body imaging," Nat. Commun. **3**, 1262 (2012).

42. K. Saito and T. Nagai, "Recent progress in luminescent proteins development," Curr. Opin. Chem. Biol. **27**, 46–51 (2015).

43. F. Zhang, L. P. Wang, E. S. Boyden, and K. Deisseroth, "Channelrhodopsin-2 and optical control of excitable cells," Nat. Methods **3**(10), 785–792 (2006).

44. Y. Hayashi, Y. Tagawa, S. Yawata, S. Nakanishi, and K. Funabiki, "Spatio-temporal control of neural activity in vivo using fluorescence microendoscopy," Eur. J. Neurosci. **36**(6), 2722–2732 (2012).

45. D. C. Klein, R. Y. Moore, and S. M. Reppert, *Suprachiasmatic nucleus: the mind's clock* (Oxford University Press, New York, 1991), pp. xvi, 467 p.

46. J. A. Mohawk and J. S. Takahashi, "Cell autonomy and synchrony of suprachiasmatic nucleus circadian oscillators," Trends Neurosci. **34**(7), 349–358 (2011).

47. S. Yamaguchi, M. Kobayashi, S. Mitsui, Y. Ishida, G. T. van der Horst, M. Suzuki, S. Shibata, and H. Okamura, "View of a mouse clock gene ticking," Nature **409**(6821), 684 (2001).

1. Introduction

In vivo BLI has been widely adopted in biological and medical research to monitor visual representations, such as gene expression, protein–protein interactions, immune, stem and cancer cells (specific tracking of cells) within living organisms [1]. BLI simply detects photons emitted from luciferin by firefly luciferase in living cells or tissues. Luciferin is a substrate for bioluminescence reaction and is oxidized in the presence of luciferase with cofactors, adenosine triphosphate (ATP) and Mg^{2+}, resulting in the formation of oxyluciferin in the spin-singlet excited state. Luminescence occurs when it returns to the ground state [2–4]. Therefore the BLI does not require excitation, and avoids background signals, the high sensitivity of BLI is owing to its high signal-to-noise ratio [5].

With conventional *in vivo* BLI, bioluminescence from cells or organs at the surface of the body can be detected through the skin and thin muscle, but bioluminescence from organs in deep tissues yields no, or much lower, signals because of the limited penetration of light, which is typically absorbed and scattered by blood and tissues. Deep areas are inaccessible to optical imaging without devices that can reach such locations.

Fiber optics has been developed for the imaging of tissues within living organisms that are inaccessible to conventional optical imaging with insertion of a miniature tip into the body with minimal physical damage [6, 7]. Bundled-fiber optics is comprised of individual step-index fibers in a closely packed arrangement and maintains the relative arrangement of individual fibers, allowing transmission of intensity images in pixelated form. Unlike lenses or gradient refractive index (GRIN) lens fibers, the fiber bundle without a lens system lacks focal capability. Instead, it takes advantage of high transmittance. Although bundled-fiber optics have already been applied in the field of fluorescence imaging *in vivo* [6–9], there have been no previous reports of BLI using bundled fibers partly because of the low transmittance and numerical aperture (NA) of previously developed fiber bundles. Recently, greater optical performance with high transmittance and density has been achieved that can detect low light signals at high resolution [10], and this method enables us to expand to BLI. We have developed a bundled-fiber-coupled microscope with a highly sensitive cooled-CCD-camera, and have successfully performed *in vivo* BLI of organs in the mouse body.

For reflectance imaging, it is necessary to efficiently reject back-reflections from the bundle end-face. This problem is resolved by placing an illumination source adjacent to the imaging optics. The scattered light from deeper tissue layers illuminates superficial tissue, and provides a vertical illumination source, resulting in images like those that would be generated from a transmittance microscope [11, 12]. This technique is useful for detecting the intrinsic optical contrast of blood vessels and structures of tissues, and allows identification of the structural details of bioluminescence image.

Here, we report *in vivo* BLI and reflectance imaging of the cerebral cortex (Cereb cortex), testis, preputial gland (Pre gla), submandibular gland (Sub gla) and a fat pad of cauda epididymis (Fat pad) in luciferase reporter mice, *Period1–luciferase* (*Per1-luc*) transgenic mice, in which the *Per1* promoter region is fused to firefly luciferase to monitor gene expression. The *Per1* gene is expressed in almost all tissues of the entire body, and one of the key molecular regulators of the circadian clock [13–16]. To our knowledge this is the first report of *in vivo* BLI in the brain and peripheral organs using bundled-fiber optics.

2. Materials and methods

2.1 Animals

Per1-luc transgenic mice (Prof. Hajime Tei, Kanazawa University and Mitsubishi Institute of Life Science) in the C57BL/6J background carrying a *Per1-luc* reporter gene, in which the *Per1* promoter region (6.7 kb) [17, 18] fused to firefly luciferase (Fluc) can be used to monitor *Per1* gene expression, were used in this study. The luciferase activity of organs in *Per1-luc* mice were evaluated by *ex vivo* luciferase assay. Bioluminescence intensity per protein of each organ is shown in Fig. 7 Appendix 1. The high bioluminescence intensity from Pre gla and testis were detected. Much lower, but still significant, bioluminescence intensities were detected from multiple organs.

Mice (male, 2 – 6 months old, body weight 25 – 35 g) were maintained under controlled environmental conditions with a room temperature of $22 \pm 2°C$, housed in cages with food and water available ad libitum under specific pathogen-free (SPF) conditions (Precision Air Processor, PAP01B; Orion, Suzuka-shi, Nagano, Japan), and entrained to a 12:12 h light/dark cycle (lights on 22:00 – 10:00, light intensity approximately 100 lux) for more than 2 weeks before the experiments. The experiments were performed at Zeitgeber Times 14 – 18 (ZT 14 – 18, where ZT 0 indicates the time of lights on), because the peak time of *Per1* gene expression in the peripheral organs is at subjective night time [19–21]. Mice were anesthetized with 30% urethane solution (1.5 g/kg body weight, i.p. injection). The hair around the target organs was trimmed. The skin was cut for observation by bundled-fiber-coupled microscopy. For imaging of Cereb cortex, the skull was ground around the target area with a dental drill (Minitor JET II, UC230; Urawa, Kuki-shi, Saitama, Japan) and a hole was opened.

This study was carried out in strict accordance with the Care and Use of Laboratory Animals of Toyohashi University of Technology. The protocol was approved by the Animal Research Committee of Toyohashi University of Technology (Permit number: DO26-6). All surgical procedures were performed under urethane anesthesia, and every effort was made to minimize suffering. The mice were euthanized after the experiments immediately.

2.2 Cultured cells

ffLuc-cp156 (ffLuc) [22] (Prof. Atsushi Miyawaki, RIKEN and Prof. Hideyuki Okano, Keio University) was made from a yellow variant of Aequorea GFP fused to firefly luciferase with extremely strong bioluminescence for higher resolution of cellular imaging. ffLuc was transfected using Lipofectamine 3000 transfection reagent (Thermo Fisher Scientific, Waltham, MA) into cultured HEK293 cells. HEK293 cells expressing ffLuc (ffLuc-HEK293 cells) were selected by G418 (1 mg / ml, 072-05182; Wako, Chuo-ku, Osaka, Japan) and stable cells, but not of a single colony, were obtained.

2.3 Experimental setup of the bundled-fiber-coupled microscope

We have developed a bundled-fiber-coupled microscope with a highly sensitive cooled-CCD-camera capable of *in vivo* BLI and reflectance imaging. The fiber bundle is constructed of 54000 single fibers each being 1.8 μm in diameter; the distance between indivisual fibers is 2.4 μm, and the tip of the fiber bundle is 600 μm in diameter as shown in Fig. 1(A). The NA value of the fiber bundle is 0.73. A high-magnification examination of the fiber bundle (inset of Fig. 1(A)) showed that indivisual fibers are arranged in a close-packed structure. The

lateral optical resolution of the fiber bundle, determined by the core-to-core distance, is 2.4 μm.

Figure 1(B) shows the bundled-fiber-coupled microscope system, which consisted of an objective lens (× 20, NA 0.5) and a tube lens (f = 180) optically coupled to the fiber bundle (DP-SMD002; Denkosha, Hamamatsu, Shizuoka, Japan) and a cooled-CCD camera (–90 ± 5°C, iXon; Andor Technology, Belfast, Northern Ireland, UK). The focal plane of the objective lens was optically conjugated with the facial side of the fiber bundle, which makes contact with the target organ surface. Fiber optics deliver light, which allows for use as the light source. For reflectance imaging, a 405 nm (DL405-050-O; CrystaLaser LC, Reno, NV) or 488 nm (DL488-050; CrystaLaser LC) laser optically coupled to a fiber (DP-SMT002; Denkosha) was used as the light source to illuminate the specimen plane. Fibers were operated to three directions by the xyz stage. The setup, except for the lasers and PC, was placed in a dark box.
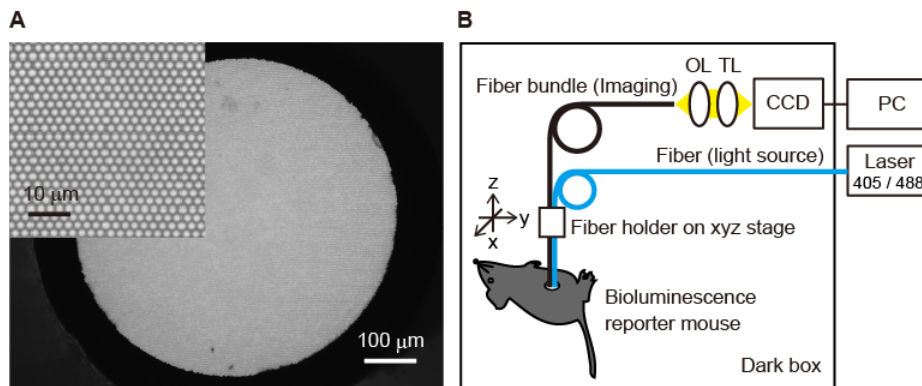

Fig. 1. The bundled-fiber-coupled microscope system. (A) Cross-sectional view of the fiber bundle. The inset shows an enlarged view. (B) Setup of the bundled-fiber-coupled microscope for *in vivo* BLI and reflectance imaging. The focal plane of the objective lens is optically conjugated with the facial side of a fiber bundle that contacts the surface of the target organ. A laser optically coupled to a fiber is used as the light source for reflectance imaging. OL: Objective lens, TL: tube lens.

2.4 Spatial resolution of the bundled-fiber-coupled microscope

Fluorescent beads 10 μm in diameter (10 – 15 μm, FluoSpheres polystyrene microspheres, orange fluorescent 540 nm/560 nm, F8833; Molecular Probes, Eugene, OR) or 50 μm (45 – 53 μm, Fluorescent Orange Polyethylene Microspheres, UVPMS-BO-1.00 45 – 53 μm – 5 g; Cospheric, Santa Barbara, CA) were scattered on a glass-based dish coated with poly-D-lysine at a low density. The bead diameter, 10 – 15 μm, is similar to that of an ordinary cell. Fluorescent beads in air or water were excited by the fluorescence microscope (ECLIPSE Ti; Nikon, Tokyo, Japan) with a light source (Intensilight C-HGFIE; Nikon) through a band pass filter (540 nm/25 nm) as shown in Fig. 2. Luminescence imaging of a single fluorescent bead was performed by the bundled-fiber-coupled microscope through a band pass filter (630 nm/60 nm) with changing the distance, x, as shown in Fig. 2, from the bead to the facial side of the fiber bundle. The maximum intensity (average intensity of the top 0.01% pixels, 26 pixels/512 × 512 pixels) and the full width at half maximum intensity (FWHM) with changing distance were calculated from the bioluminescence image data.
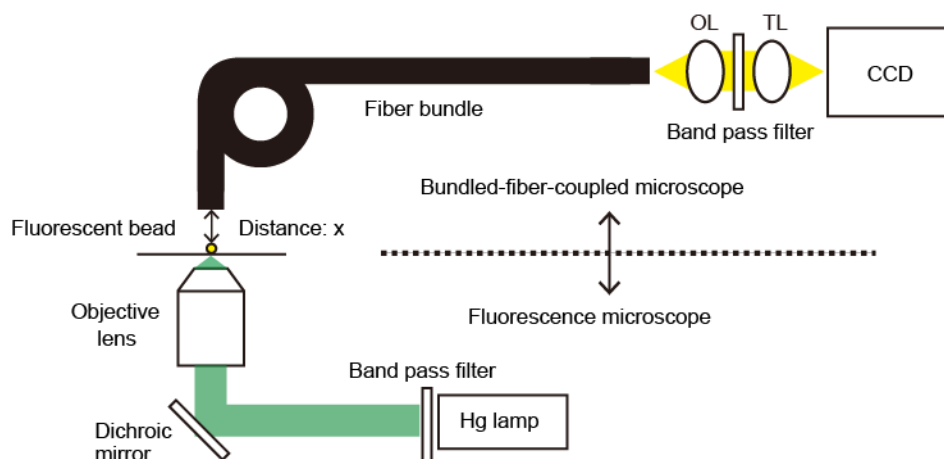
Fig. 2. Experimental setup for spatial resolution analysis of the bundled-fiber-coupled microscope. A fluorescent bead in the air or in water is excited by the fluorescence microscope system, and luminescence imaging of the fluorescence bead is performed by the bundled-fiber-coupled microscope with changing distance, x, from the bead to the facial side of the fiber bundle.

2.5 Bioluminescence and reflectance imaging

Cultured cells expressing ffLuc. ffLuc-HEK293 cells were scattered with low (2×10^5 cells) and high (1.75×10^6 cells) densities in 35 mm-culture dishes one or two days before measurement. Luciferin solution was added to the culture medium at a final concentration of 0.1 mM. The fiber bundle contacted with the surface of the cells, and reflectance imaging and BLI of the ffLuc-HEK293 cells were observed by the bundled-fiber-coupled microscope. (35 mm dish was placed on a heat block set at 37 °C). For reflectance imaging, a white-LED light placed near the dish was used as a light source instead of the illumination fiber which is illustrated in Fig. 1. Reflectance imaging and BLI were performed for integral times of 0.1 seconds and less than 5 minutes respectively.

Mouse brain and organs *in vivo*. The tip of the imaging fiber bundle and the illumination fiber were placed on the brain or peripheral organs. For reflectance imaging, a 405 nm or 488 nm laser optically coupled to a fiber was used as a light source. Reflectance imaging was performed for an integral time of less than 0.1 seconds. For BLI, 0.5 μL of 50 mM D-luciferin solution (Beetle Luciferin Potassium Salt, E1602; Promega, Madison, WI) diluted in phosphate-buffered saline (PBS) was injected by a pipette at the tip of the fiber bundle by the micropipette for each measurement. BLI was performed for an integral time of less than 5 minutes (30 seconds to 5 minutes). Bioluminescence intensity (average value of bioluminescence image within the fiber bundle area per pixel with 5minuets accumulation) of each organ were calculated. To reduce the spatial specificity of bioluminescence intensity on each organ, areas with large blood vessels were avoided.

2.6 Imaging data acquisition and analysis

Imaging data was acquired by Solis (Andor Technology), analyzed by ImageJ (NIH) and processed by Matlab (MathWorks) and Photoshop (Adobe). Data are expressed as the mean ± SE. For statistical analysis, the unpaired Student's t test was applied (GrapPad Prism6).

3. Results

3.1 Spatial resolution of the bundled-fiber-coupled microscope

The bundled-fiber-coupled microscope does not have focal capacity and lacks axial resolution, and therefore the spatial resolution in proportion to distance between the luminescent sample and the edge of the fiber bundle was measured. Fluorescent beads 10 μm

(10 – 15 µm) or 50 µm (45 – 53 µm) in diameter in the air or water were excited by the fluorescence microscope system (Fig. 2). Luminescence images of 10-µm beads with distance, x, of 0, 10, 20 and 30 µm were obtained as shown in Fig. 3(A). (The intensity range of imaging was optimized.) The diameter of the luminescence image increased proportionally to the distance. A fluorescent bead in water is more similar to the environmental conditions in a luminescent cell *in vivo* compared to that in the air, because the refractive index of a cell is similar to that of water [23, 24].

The maximum intensity with changing distance was calculated from the imaging data as shown in Fig. 3(B). (The solid and dashed lines represent the smoothed curves of data with the Gaussian kernel [SD = 2.5 µm] in the air and in water, respectively.) With 10-µm beads (Fig. 3(Bi)), the distances at half maximum in the air and in water were estimated to be 6.1 µm and 6.2 µm, respectively. The maximum intensities became 24% and 28% at a distance of 10 µm and 5% and 7% at 20 µm in the air and in water, respectively. The maximum intensity of 50-µm beads became rather flat at a distance of around 4 µm because of the size effect of the bead toward the distance as shown in Fig. 3(Bii). The distances at half maximum were estimated to be 10.5 µm and 12.5 µm in the air and in water, respectively; these values were about double those of the10-µm beads. The luminescence intensity of 50-µm beads decreased to 53% and 62% at a distance of 10 µm, 18% and 25% at 20 µm in the air and in water, respectively. The transmittance of the tissue was not considered in this system, so it would be lower in BLI *in vivo*.

FWHM (d in inset of Fig. 3C(i)) with changing distance was calculated from the imaging data as shown in Fig. 3C. FWHM was fitted by a hyperbolic function curve ($d^2 = a^2 \times x^2 + b^2$ where "a" and "b" are constants, and the cross-correlation between raw data and the predicted data was > 0.99). With 10-µm beads (Fig. 3C(i); [a, b] = [3.8, 14.4] and [2.8, 14.4] in the air and in water, respectively), FWHM was linearly proportional to distance, while it has not linearly related to distance when the distance approached 0 µm. If an ideal point light source could be used, FWHM would become 0 µm at a distance of 0 µm. However, the size of the fluorescent bead cannot be ignored. Within distances < 4 µm, FWHM became almost constant. The distances at which FWHM doubled were calculated as 6.6 µm and 8.9 µm in the air and in water, respectively. The nearest neighbor beads would not be distinguishable with longer distance than the distance at which FWHM doubled. With 50-µm beads (Fig. 3(Cii); [a, b] = [4.2, 44.2] and [3.1, 43.3] in the air and in water, respectively), FWHM became almost constant within a distance < 7 µm, which was slightly larger than that of 10-µm beads. The distances at which FWHM doubled were calculated as 18.4 µm and 24.2 µm in the air and in water, respectively. Density (bead-to-bead distances), size, luminescent intensity of beads, and depth of the bead location would determine whether the luminescence signal of each bead could be identified separately.
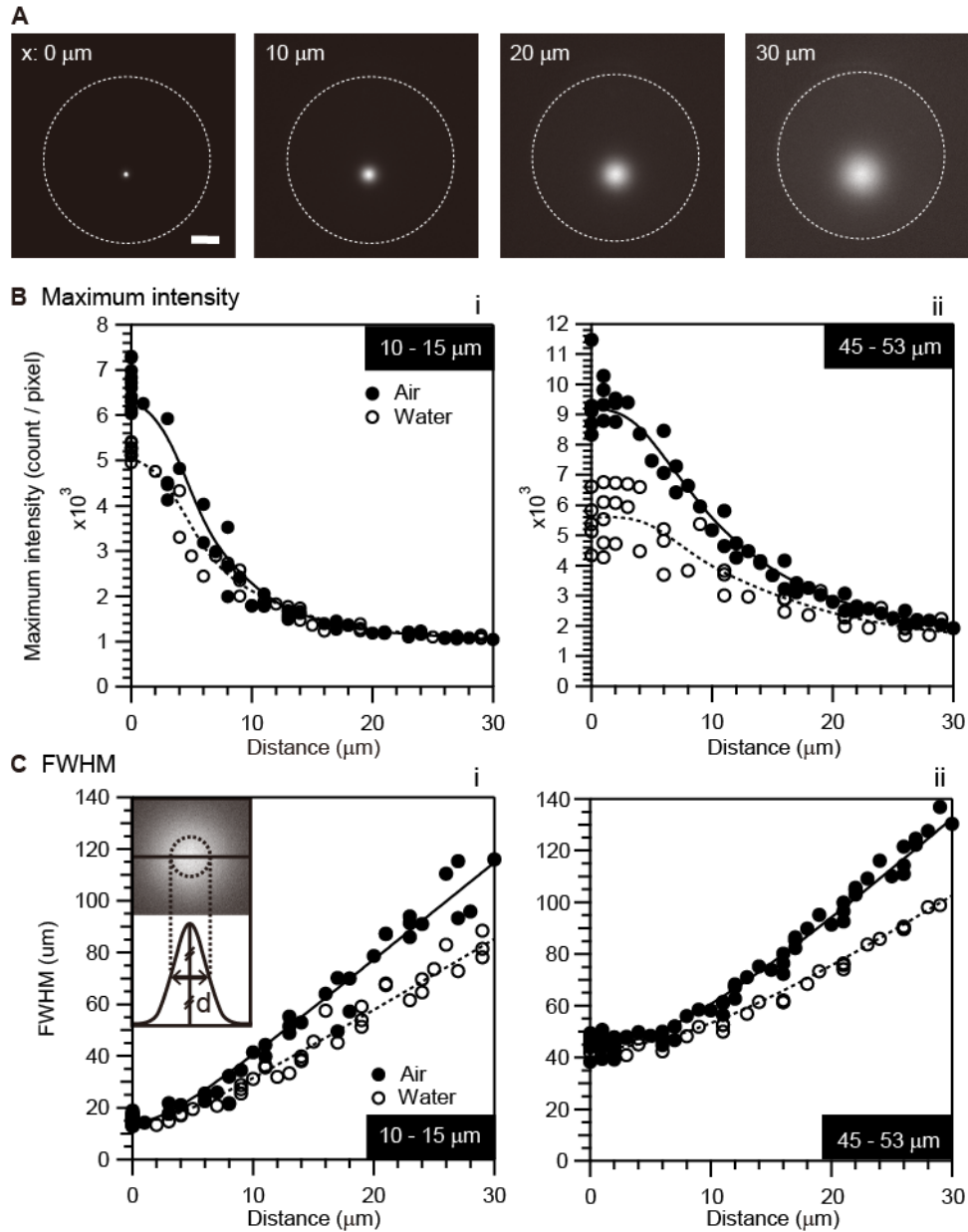
Fig. 3. Spatial resolution of the bundled-fiber-coupled microscope. (A) Luminescnce images of a single fluorescent bead, 10 – 15 μm in diameter, with changing distance, x = 0, 10, 20 or 30 μm. The dashed circle indicates the edge of the fiber bundle. The scale bar indicates 100 μm. (B) The maximum intensity with changing distance (i: 10 – 15 μm bead, ii: 45 – 53 μm bead). The closed circle indicates in the air and the opened circle indicates in water. The solid and dashed lines represent the smoothed curves of data with the Gaussian kernel (SD = 2.5) in the air and in water, respectively. (C) FWHM (d) in diameter of luminescence image with changing distance (i: 10 – 15 μm bead, ii: 45 – 53 μm bead). The closed circle indicates in the air and the opened circle indicates in water. Both are fitted by a hyperbolic function curve with a solid curve and a dashed curve for air and water, respectively. The inset shows the concept of FWHM, d.

3.2 Bioluminescence and reflectance imaging

Cultured cells expressing ffLuc. We successfully observed BLI and reflectance imaging of ffLuc-HEK293 cells by the bundled-fiber-coupled microscope as shown in Fig. 4. (The intensity range of each image was optimized.) Cultured cells exist as a one cell layer. As the spatial resolution 2.4 μm of the fiber bundle was enough to recognize a single cell, cells with low density were observed in a single-cell level as shown in Fig. 4(a1) and 4(a2). With increasing the cell density, the cells exist touching each other and make the structure like clusters as shown in Fig. 4(b1) and 4(b2). In this case, it needs more than a 2.4 μm space between each cell to distinguish them.
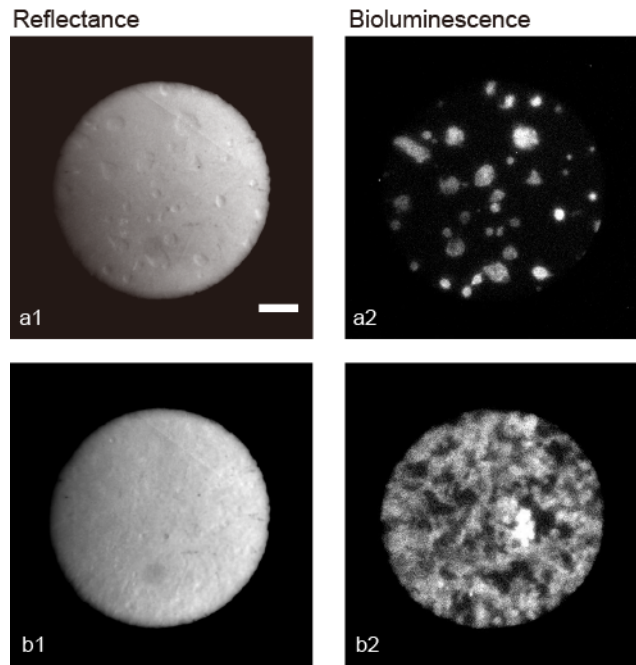
Fig. 4. Bioluminescence and reflectance images of ffLuc-HEK293 cells. Reflectance image (left) and bioluminescence image (right) with high (upper) and low (bottom) cell densities. The scale bar indicates 100 μm.

Mouse brain and organs *in vivo*. BLI and reflectance imaging of Cereb cortex, testis, Pre gla, Sub gla, and Fat pad of *Per1-luc* mice were observed at ZT 14 – 18 as shown in Fig. 5. Reflectance imaging with 405 nm and 488 nm laser illumination are shown in the left column of Fig. 5 and Fig. 8 Appendix 2, respectively. As the illumination fiber was adjacent to one side of the imaging fiber and illumination was position-dependent, the intensity trend (shade) of non-uniform illumination was eliminated by subtraction of the inverse square function derived by least square fitting. The structure of blood vessels could be seen clearly with illumination at 405 nm (left column in Fig. 5, because 405 nm is in the wavelength range of hemoglobin absorption [25]. On the other hand, with 488 nm illumination, the blood vessels could not be seen clearly (see Fig. 8, Appendix 2) because of the much lower absorption by hemoglobin. However, overlapping blood vessels could be clearly identified (indicated by a triangle in Fig. 8, Appendix 2) better than with 405 nm illumination (Fig. 5(a1)).

BLI was performed with a exposure time from 30 seconds to 5 minutes with injection of 0.5 μL of 50 mM luciferin as shown in the middle column of Fig. 5. Superposition of reflectance images in grayscale and bioluminescence images in heat maps with 16 colors in lookup tables of ImageJ are shown in the right column of Fig. 5. The intensity range of each reflectance and bioluminescence image was optimized. The structures of blood vessels could be seen clearly with 405 nm light illumination in Cereb cortex and testis (Fig. 5(a1) and 5(b1)

respectively). Bioluminescence images could also be obtained (Fig. 5(a2) and 5(b2) respectively). On comparison between the reflectance and bioluminescence images, the dark (low bioluminescence intensity) area observed in the bioluminescence image could be identified as blood vessels in the superposition images (Fig. 5(a3) and 5(b3) respectively).

In Pre gla, the structure of blood vessels could also be seen clearly as shown in Fig. 5(c1). In BLI (Fig. 5(c2)), some elliptical bioluminescent structures several tens to a hundred micrometres in size were observed. As shown in the superposition image (Fig. 5(c3)), the dark area in the bioluminescence image partly coincided with the structure of blood vessels, although the correspondence was not exact. The dark area in bioluminescence images could even be seen in regions that did not have clear blood vessels. Therefore, these bioluminescent structures (cells) were present in the organ. We performed fluorescence imaging of Pre gla with fluorescent staining of the cell membrane by the confocal microscope system (A1; Nikon) as shown in Fig. 9, Appendix 3. Appendix 3 show the perspective and the magnified fluorescence image of the cell membrane in Pre gla, respectively. The characteristic structure and size of the cell membrane corresponded to cells constituting Pre gla [26]. The elliptical bioluminescent structures observed in Fig. 5(c2) were similar in size to cells, which suggested that the bioluminescence from cells of Pre gla was observed. It would be better to obtain both bioluminescence and fluorescence images with the bundled-fiber-coupled microscope to allow a precise comparison, but this was not possible in the present study because our setup without the excitation system was specific to BLI. We also measured the bioluminescence and reflectance images of Sub gla and Fat pad as shown in Fig. 5(d) and 5(e) respectively. The structure of blood vessels was seen in Sub gla and Fat pad. Not only the structure of blood vessels but also the characteristic structure of the tissue was observed in Fat pad. Bioluminescence images of Sub gla and Fat pad were also obtained.
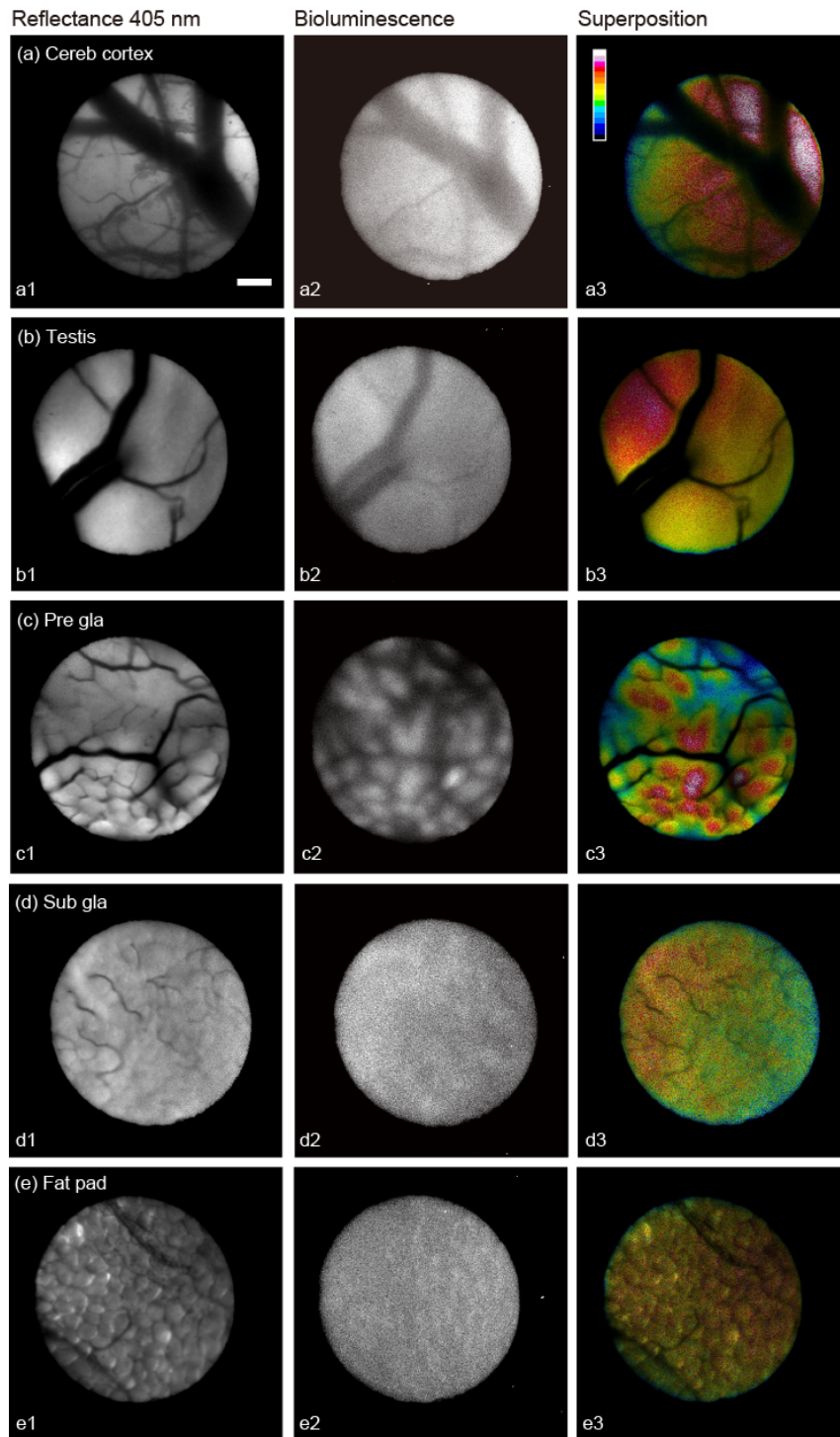
Fig. 5. *In vivo* bioluminescence and reflectance image of the brain and peripheral organs of *Per1-luc* mice. Bioluminescence and reflectance image of Cereb cortex (a), testis (b), Pre gla (c), Sub gla (d), and Fat pad (e) of *Per1-luc* mouse. (Left) Reflectance images with 405 nm illumination. (Middle) Bioluminescence images. (Right) Superposition image of the reflectance image in grayscale and the bioluminescence image as a heat map with 16 colors in lookup tables of ImageJ. The scale bar indicates 100 μm.

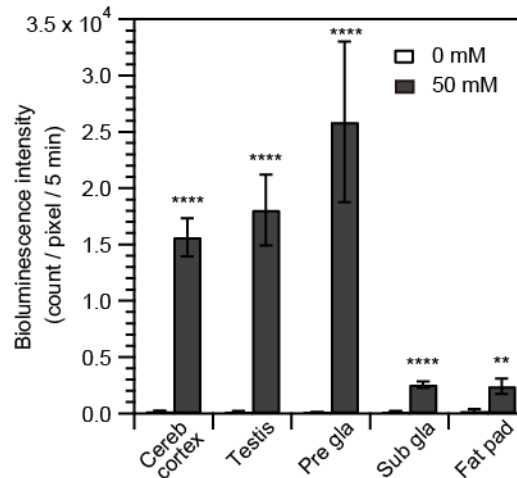Bioluminescence intensity from images of each organ were calculated as shown in Fig. 6. The data show the mean intensity per pixel for an integral time of 5 minutes $\pm$ SE (Cereb cortex, 15636 $\pm$ 1680, $n = 7$; testis, 18063 $\pm$ 3141, $n = 6$; Pre gla, 25878 $\pm$ 7144, $n = 7$; Sub gla, 2553 $\pm$ 292, $n = 7$; Fat pad, 2415 $\pm$ 673, $n = 6$ with 50 mM luciferin and Cereb cortex, 198 $\pm$ 42, $n = 4$; testis, 166 $\pm$ 63, $n = 4$; Pre gla, 109 $\pm$ 11, $n = 4$; Sub gla, 192 $\pm$ 28, $n = 4$; Fat pad, 236 $\pm$ 153, $n = 3$ with 0 mM luciferin; ****$p < 0.0001$; **$p < 0.01$ vs. the mean intensity with 0 mM luciferin of each organ, unpaired Student's t test). Similar to the result of *ex vivo* luciferase assay (see Appendix 1), high bioluminescence intensities of Cereb cortex, testis, and Pre gla were observed compared to Sub gla and Fat pad.

Fig. 6. Bioluminescence intensity. The data show the mean intensity per pixel for an integral time of 5 minutes $\pm$ SE (Cereb cortex, 15636 $\pm$ 1680, $n = 7$; testis, 18063 $\pm$ 3141, $n = 6$; Pre gla, 25878 $\pm$ 7144, $n = 7$; Sub gla, 2553 $\pm$ 292, $n = 7$; Fat pad, 2415 $\pm$ 673, $n = 6$ with 50 mM luciferin, and Cereb cortex, 198 $\pm$ 42, $n = 4$; testis, 166 $\pm$ 63, $n = 4$; Pre gla, 109 $\pm$ 11, $n = 4$; Sub gla, 192 $\pm$ 28, $n = 4$; Fat pad, 236 $\pm$ 153, $n = 3$ with 0 mM luciferin; ****$p < 0.0001$; **$p < 0.01$ vs. the mean intensity with 0 mM luciferin, unpaired Student's t test).

4. Discussion

We have developed a bundled-fiber-coupled microscope capable of *in vivo* BLI and reflectance imaging in the body, and successfully detected cellular signals from the brain and peripheral organs of bioluminescence reporter mice, *Per1-luc* mice. With conventional *in vivo* BLI (e.g., IVIS Imaging System; PerkinElmer, Waltham, MA), only the bioluminescence from organs at the surface can be detected through the skin and thin muscle, while that from deep organs yields no, or much lower, signals [1, 27]. Although the bioluminescence images of whole organs could be obtained, the micro-level structural details of the organ were unrecognizable. Usually, luciferin solution is injected (e.g., 15 mg/kg body weight [28]) intraperitoneally (i.p.), intravenously (i.v.) or subcutaneously (s.c.), and therefore a large amount of luciferin would be needed to obtain signals. There are problems associated with the time dependence of luciferin concentration in the target organ due to diffusion and metabolism in the body [28–30]. Therefore, bioluminescence images from organs should be obtained with careful time control and signal acquisition should be performed at the optimal time. Conventional systems have the advantage of being non-invasive and suitable for long-term measurement.

On the other hand, the bundled-fiber optics system allows *in vivo* BLI of cells or organs at deep sites in the body of a living organisms. This system yields bioluminescence images from a part of the organ that is determined by the diameter of the fiber bundle. In our system, the observation view is 0.28 cm^2. Using fiber bundle with larger size of tip, it is possible to have a wider view of imaging. However with increasing the diameter of the fiber bundle, it would

decrease flexibility causing difficulty in handling. To avoid this problem, using a plastic fiber bundle with a large tip size is another approach. The plastic fiber has an advantage in flexibility, and recently their spatial resolution and optical performance have been improved. Generally plastic fiber optics have auto fluorescence, and it is not suitable for fluorescence imaging with a certain excitation wavelength. As bioluminescence imaging does not need excitation, it is available. Only a small amount of luciferin solution (0.5 μL of 50 mM luciferin) needs to be injected at the tip of the fiber bundle for each measurement. Bioluminescence was little influenced by the diffusion and metabolism of luciferin in the body. This time we used a micropipette to inject luciferin solution. However, when much deeper tissue in the body needs to be observed, a method of injection that uses a thin tube along the fiber bundle would be required [31].

With reflectance imaging, the structural details of blood vessels and organs could be recognized (Fig. 5, Appendix 2). It allows identification of the structural details observed in the bioluminescence image. We adopted a simple illumination scheme where the illumination fiber was placed adjacent to one side of the imaging fiber bundle. It had the intensity trend of non-uniform illumination. In addition, the size of the end portion (imaging fiber bundle and illumination fiber) was not small enough to insert into a deeper site in the body. It would be user friendly to adopt a uniform and compact illumination scheme [31–34].

As the bundled-fiber-coupled microscope does not have focal capacity and lacks axial resolution, we performed a spatial resolution analysis of this system. The maximum intensity and FWHM of fluorescent beads are correlated with the distance (Fig. 3(B) and 3(C)). It is determined by density, size, luminescent intensity of target, and depth (distance) from the end-face of the fiber bundle besides the lateral resolution of the fiber bundle, as to whether luminescence signal of each can be recognized separately. We could not determine to what depth it is possible to detect bioluminescence signals, because the absorption (membrane permeability) and diffusion of luciferin at specific depths within each organ could not be estimated. Merged luminescence signals from several cell layers at depth would result in lower resolution in luminescence images. In Cereb cortex and testis, the bioluminescence seemed rather uniform but not at cellular resolution (Fig. 5(a2) and 5(b2) respectively). In Pre gla, the size of bioluminescent cells ranged from several tens to a hundred micrometers. Bioluminescence signals from neighboring cells in both lateral and axial directions were not merged, and each cell could be identified separately (Fig. 5(c2)). With a lens system, such as the GRIN lens and confocal system [35–39], it may be possible to observe the bioluminescence from cells at a higher resolution. However, it is necessary to take into consideration the reduced transmittance. Taking bioluminescence imaging with two (or more) fiber bundles which confront at a certain degree at their tips, bioluminescence-topography-like imaging would be available. This tomographic information could evaluate the spatial resolution in depth more precisely.

Although the applicability of bundled fiber imaging has already broadened to *in vivo* fluorescence imaging, BLI has not been reported. Here, we successfully showed that bundled-fiber optics enabled BLI *in vivo* by fiber bundles. The advantage of fluorescence imaging is higher brightness, which enables the visualization of a target at a cellular or sub-cellular level in a millisecond time scale. The lack of requirement for substrate and cofactors is also advantageous. The disadvantage of fluorescence imaging is an auto-fluorescence, the photo-induced damage of tissues in the body, and photo-bleaching of the probe. On the other hand, the benefit of BLI is the low background, and high signal-to-noise ratio in comparison with fluorescence imaging [5]. Despite its advantages, BLI had not used because of its dimness. Influencing factors (e.g., substrate, cofactors, and enzyme inhibitors) in the bioluminescence reaction should be kept in mind, and controled when performing *in vivo* BLI [27].

Recently to overcome the problem of dimness, a brighter luciferase substrate with synthetic analogues, and a bioluminescent reporter system, which enables near realtime imaging, have been developed [22, 40–42]. In addition, BLI is especially useful when applied along with optical stimulation techniques, such as channelrhodopsin-2 (ChR2) [43], to control neural activity, instead of fluorescence imaging, which requires excitation with light. It is

available for not only observing signals, but also for photoactivating ChR2-expressing cells with high resolution in a living animal [44]. With these new techniques, BLI has become indispensable to monitor biological phenomena. The importance of the BLI technique is increasing, and the bundled-fiber-coupled microscope could be applied for such studies. Basic research on biological processes would benefit from instrumentation that permits cellular imaging that is not possible with conventional systems (e.g., in hollow tissue tracts), and such methods could be applied to clinical diagnostics and surgical procedures in a low invasive manner.

In this study, we obtained *in vivo* bioluminescence images of *Per1-luc* mice. The molecular clock is believed to be mediated by an autoregulatory transcription and translation feedback loop of the circadian clock gene expression (e.g., *Per1*) [15]. The circadian rhythms, with nearly 24-hour periodicity, in mammalian physiology and behavior are regulated by the coordination of a central pacemaker located in the hypothalamic suprachiasmatic nucleus (SCN) [45, 46]. As a long-term recording, *in vivo* BLI from the brain would be available. A flexible fiber optic device allows imaging in a freely moving animal. *In vivo* bioluminescence measurement of the SCN in free-moving *Per1-luc* mice using a single fiber coupled to a photomultiplier has already been reported [47]. However, BLI has not yet been reported. Therefore, BLI of SCN in a free-moving mouse with measurement of other physiological parameters (e.g., behavior) would advance the functional analysis of the mammalian circadian mechanism.

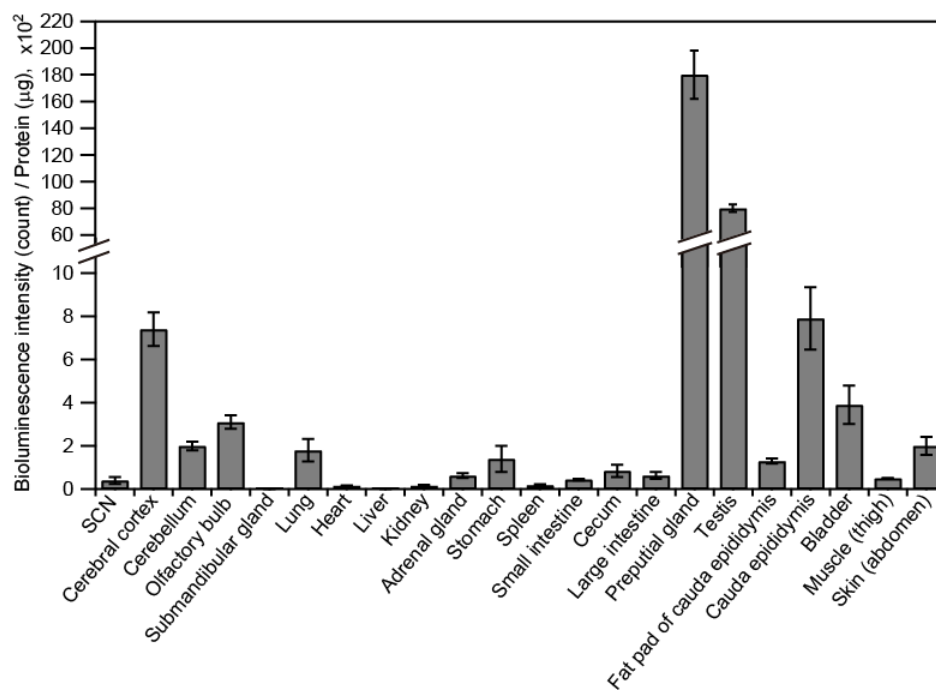**Appendix 1: Ex vivo luciferase assay of Per1-luc mouse**

Fig. 7. *Ex vivo* luciferase assay of *Per1-luc* mouse. Luciferase activity in the brain and organs of *Per1-luc* mice were evaluated by *ex vivo* luciferase assay. Each organ was cut into small pieces and homogenized. The supernatant from each sample were mixed with luciferase assay kit (PicaGene BrillianStar-LT, 301-15371; Toyo Ink Group, Tokyo, Japan). Bioluminescence intensity was measured with a plate reader (Fluoroscan Ascent FL; Thermo Scientific). The protein concentration of the supernatant was determined with a BCA protein assay kit (Pierce BCA Protein Assay Kit, 23227; Thermo Scientific), and used to correct the bioluminescence intensity. Bioluminescence intensity per protein of each organ is plotted (mean ± SE, n = 4 except Sub gla and Fat pad n = 3).

Appendix 2: Reflectance image with 488 nm illumination
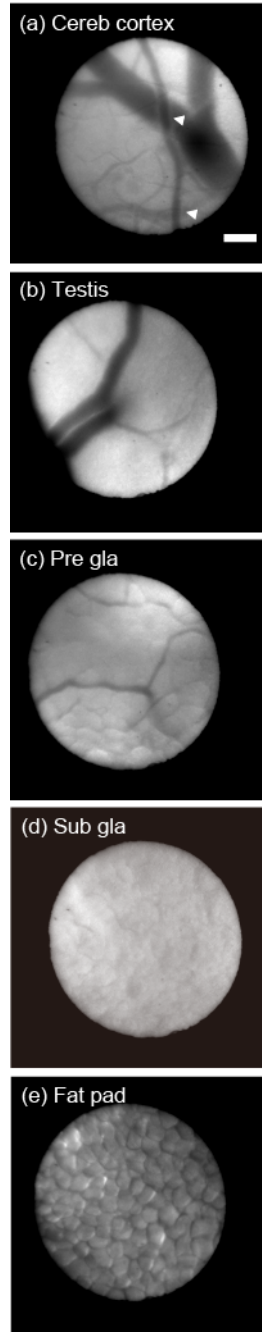
Reflectance 488 nm

Fig. 8. Reflectance image with 488 nm illumination. Reflectance images with 488 nm illumination of Cereb cortex (a), testis (b), Pre gla (c), Sub gla (d), and Fat pad (e) of *Per1-luc* mouse. Triangles in (a) show the overlapping of blood vessels. The scale bar indicates 100 μm.

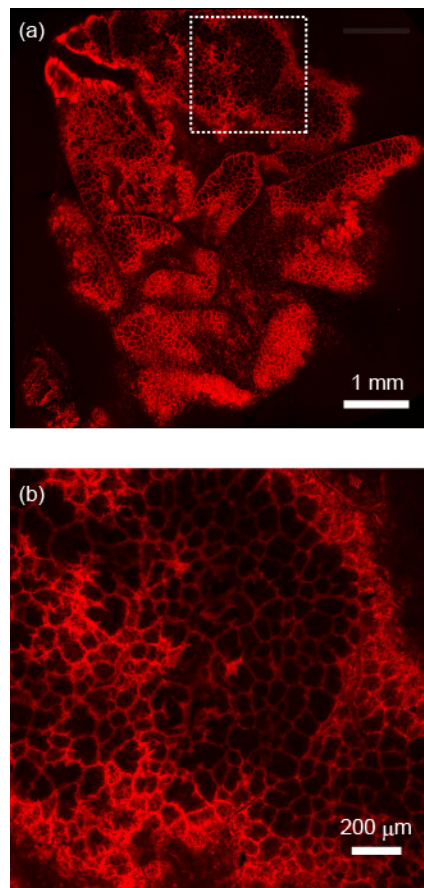**Appendix 3: Fluorescence imaging of cell membrane in Pre gla**

Fig. 9. Fluorescence imaging of cell membrane in Pre gla. Pre gla was fixed and stained with the fluorescent marker for the cell membrane (CellMask Deep Red plasma Membrane Stain, C10046, diluted 1:2000 with PBS; Molecular Probes, Eugene, OR). Fluorescence imaging was performed using a confocal microscopy system (A1; Nikon). (a) and (b) show the perspective and magnified fluorescence image, respectively.

Acknowledgments